$La_{0.6}Sr_{0.4}Co_{0.8}Ga_{0.2}O_{3-\delta}$ (LSCG) Hollow Fiber Membrane Reactor: Partial Oxidation of Methane at Medium Temperature

Yasotha Kathiraser and Sibudjing Kawi
Dept. of Chemical and Biomolecular Engineering, National University of Singapore, Singapore, 117576

DOI 10.1002/aic.14202
Published online August 23, 2013 in Wiley Online Library (wileyonlinelibrary.com)

In this study, $La_{0.6}Sr_{0.4}Co_{0.8}Ga_{0.2}O_{3-\delta}$ (LSCG) hollow fiber membrane reactor was integrated with Ni/$LaAlO_3$-Al_2O_3 catalyst for the catalytic partial oxidation of methane (POM) reaction. The process was successfully carried out in the medium temperature range (600–800°C) for reaction of blank POM with bare membrane, catalytic POM reaction and swept with H_2:CO gas mixture. For the catalytic POM reaction, enhancement in selectivity to H_2 and CO is obtained between 650–750°C when O_2:CH_4 <1. High CH_4 conversion of 97% is achieved at 750°C with corresponding H_2 and CO selectivity of about 74 and 91%. The oxygen flux of the membranes also increased with the increase in oxygen partial pressure gradient across the membrane. The postreacted membranes were tested via XRD and FESEM-EDX for their crystallinity and surface morphology. XPS analysis was further used to investigate the O1s, Co 2p and Sr 3d binding energies of the segregated elements from the reducing reaction environment. *AIChE J*, 59: 3874–3885, 2013
Keywords: catalytic hollow fiber membrane reactor, partial oxidation of methane (POM), integrated separation-reaction, elemental analysis

Introduction

Synthesis gas (syngas) production (a mixture of H_2 and CO) is important in chemical industries as it can be easily converted to chemicals and fuels (via Fischer-Tropsch synthesis) and used for hydrogen production.[1,2] Production of syngas via catalytic hydrocarbon conversion reactions such as partial oxidation of methane (POM), and steam reforming of methane (SRM), have been widely investigated since CH_4, the main component of natural gas, is readily accessible.[3] The POM reaction appears to be an attractive alternative to SRM for hydrogen production due to its mild exothermicity, as compared to the highly endothermic nature of the SRM reaction which renders it a capital and energy intensive process.[4] The main difficulty for POM reaction, however, stems from the requirement of the costly cryogenic air separation process for oxygen supply.[5]

Several research developments focusing on integrated catalytic membrane reactor systems with mixed ionic and electronic conducting (MIEC) membranes capable of selective oxygen production from air have been carried out.[6–11] The synergic effects of coupling separation and reaction in a single unit are expected to play a decisive role in the area of sustainable energy technologies by allowing a process design without the cost intensive (cryogenic) oxygen separation unit.[12,13] Hence, the optimal process design can minimize energy consumption.[14]

According to Balachandran et al.[6] direct contact of the membrane with the reducing gases of H_2 and CO from the reaction may cause the oxide phase to lose the lattice oxygen, resulting in decomposition of the perovskite structure. Hence, immediate replenishment of the lattice oxygen through thinner wall structure is crucial. In this regard, hollow fiber membrane configuration has distinct advantages over disc or tubular membranes as it can provide larger area per unit volume and enables facile high-temperature sealing.[15]

Despite structural optimization, phase decomposition of membranes under syngas producing conditions is a prevalent issue due to the large oxygen partial pressure gradient from the air and permeate (reaction) side. Since Teraoka et al.[16] first reported on perovskite oxides such as $La_xSr_{1-x}Co_yFe_{1-y}O_{3-\delta}$ with high-oxygen permeability, cobalt-based perovskite materials have been widely investigated.[17,18] However, Co-based materials are also known for their limited chemical stability.[19] Pei et al.[20] reported the failure mechanism on $SrCo_{0.8}Fe_{0.2}O_x$ (SCFO) membranes which fractured under POM conditions due to crystal lattice mismatch caused by high-oxygen chemical potential gradient across the membrane. In order to improve the stability of membrane materials, cations with constant valence (Zr^{4+}, Ga^{3+} and Al^{3+}) were used as a partial substitution for the B-site cations (Co^{4+}/Co^{3+} and/or Fe^{4+}/Fe^{3+}).[19,21,22]

We have recently tested the Ga-doped $La_{0.6}Sr_{04}Co_{0.8}Ga_{0.2}O_{3-\delta}$ (LSCG) hollow fiber membranes for CO_2 stability with intermittent exposure to CH_4 and He as sweep gas.[23] Therefore, in this contribution, we explore the feasibility of incorporating a Ni based catalyst and assembling a LSCG catalytic hollow fiber membrane reactor for POM reaction.

Correspondence concerning this article should be addressed to S. Kawi at chekawis@nus.edu.sg.

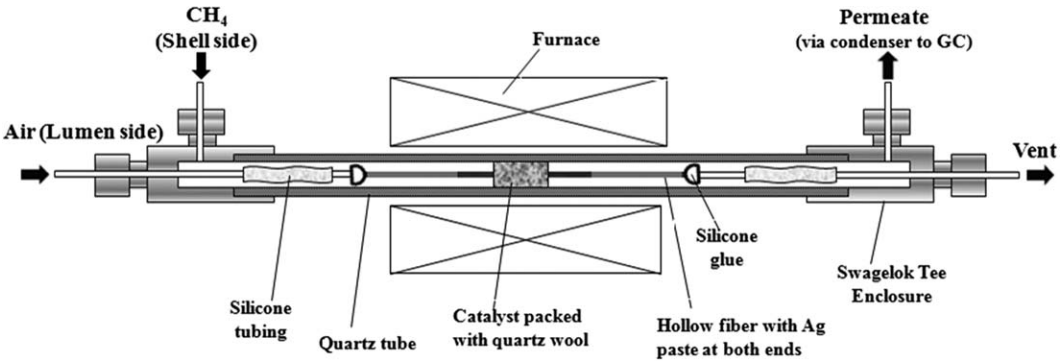

Figure 1. Schematic for catalytic LSCG membrane reactor setup.

Valuable insights on the morphological changes which took place on the membrane surface upon POM reaction, as well as upon exposure to H_2 and CO gases are discussed based on data from elemental analysis techniques such as energy dispersive spectroscopy (EDX) and X-ray photoelectron spectroscopy (XPS). The medium temperature range of 600 to 800°C was chosen for study since a suitable operation temperature is an important criterion for POM reaction. The reason being, too low a temperature leads to insufficient oxygen permeation, thereby limiting the methane conversion, whereas too high a temperature leads to deep oxidation thus compromising on product selectivity.[24] Furthermore, too high a temperature also results in catalyst sintering and deactivation which is not practical for the system.[9] Based on the results of POM reaction, the possible reaction pathways were postulated and compared with previous studies which were mainly conducted at 800°C and above.

Experimental

LSCG hollow fiber membrane fabrication

The $La_{0.6}Sr_{0.4}Co_{0.8}Ga_{0.2}O_{3-\delta}$ (LSCG) composite perovskite was synthesized via an ethylene glycol- citric acid complexation method as decribed in our previous study.[23] Citric acid (CA) (99.5+%, Merck) was dissolved in ethylene glycol and water. Lanthanum(III) nitrate hydrate (99.9%), strontium nitrate, cobalt(II) nitrate hexahydrate and gallium(III) nitrate hydrate (99.9%) were purchased from Sigma Aldrich. The composite material was further calcined at 950°C for 5 h to obtain the perovskite phase. Thereupon, the dense LSCG perovskite hollow fiber membranes were fabricated by phase-inversion spinning process as prescribed in our previous work.[23] A mixture consisted of LSCG powders, poly (ether sulfone) (PESf, Radel A-300, Ameco Performance) and N-methyl-2-pyrrolidone (NMP, Merck) were mixed in a ratio of 1:4:9 (mass ratio). Upon stirring for 72 h, the solution was degassed prior to spinning. A spinneret with the orifice diameter/inner diameter of 2.4/1.1 mm was applied to form the hollow fiber precursors. 75% DI water-25% NMP and tap water were used as the internal and external coagulants, respectively. The green membranes were sintered at 1750°C for 5 h to obtain gas-tight hollow fiber membranes. Upon sintering, hollow fibers with inner diameter about 800 μm, and wall thickness about 170 μm (with a dense layer about 80 μm), were obtained. The length of hollow fiber membrane before sintering is about 33 cm, and after sintering is about 23 cm. Hence, the membrane shrinkage is about 30%.

Catalyst preparation

1.48 g of $La(NO_3)_3.6H_2O$ (Sigma Aldrich) were added to 1.5 g of γ-Al_2O_3 (Merck). The reactants were dissolved in the appropriate molar ratios in DI water and stirred and heated to 55°C. Upon drying, the catalyst support was placed in an oven and left to dry overnight at 100°C. A calcination temperature of 900°C for 6 h was then employed to facilitate the solid-state diffusion for perovskite phase to form $LaAlO_3$-Al_2O_3 structure. 5 wt % Ni was then impregnated on the $LaAlO_3$-Al_2O_3 supports and upon drying overnight, the catalyst was calcined at 400°C for 1 h (for nitrate decomposition) and further to 600°C for 5 h.

POM reaction and sweep with H_2:CO gas mixture

Figure 1 shows the schematic of the catalytic membrane reactor setup. Two ends of the sintered fiber were adhered by silicone glue (Dow Corning) to quartz tube. 0.2 g of a Ni based catalyst developed by our research group (% Ni/$LaAlO_3$-Al_2O_3) was spread on the quartz wool packed around the hollow fiber in the midsection corresponding to the optimal heated length in the furnace, which has a total length of 15 cm (Carbolite MTF 10/15/130/3216P1). For the blank POM reaction with only the bare membrane, the same configuration was used except that no catalyst was packed.

The 5% Ni/$LaAlO_3$-Al_2O_3 catalyst was first prereduced under H_2 flow at 600°C for 30 min. Silver paste was coated on all parts of the membrane surface except 4.5 cm of the midsection which is the approximated length of the optimal heating zone of the furnace. The purpose of coating the Ag paste on the external surface of the membrane (apart from the central heated area) was to create a barrier to minimize permeation from other parts which are not within the central heating zone. Hence, in this way, a more accurate estimation of the O_2 flux from POM reaction can be determined. Air flow rate of 100 mL min^{-1} was introduced to the lumen side, whereas the reactant was introduced on the shell side (25% CH_4/He, 10 mL min^{-1}). The furnace was heated up from room temperature to 600°C at a rate of 2.5°C min^{-1}. POM reaction testing was conducted at the interval of 25°C and held for 3 h for each interval. Reaction testing was carried out in the medium temperature regime of 600 to 800°C. In order to calculate the reactant conversion and products in the effluent stream, the shell-side gas outlet was connected to a gas chromatography (GC6890N, Agilent), and analyzed by a thermal conductivity detector (TCD) using a Hayesep D 100/120 column. For the exposure to 50% H_2:CO gas

mixture (in helium), the sweep gas in the shell side consists of 2.5 mL min^{-1} H_2, 2.5 mL min^{-1} CO and 5 mL min He^{-1}. Air was introduced at a rate of 100 mL min^{-1} in the lumen side and the experiment was conducted in the same way as the POM reaction.

The conversion of CH_4 (X_{CH_4}), selectivity of CO (S_{CO}), and H_2 (S_{H_2}), and the O_2 permeation flux (J_{O_2}) are defined, respectively as follows[25]

$$X_{CH_4}(\%) = \frac{F_{CH_4,in} - F_{CH_4,\text{out}}}{F_{CH_4,in}} \times 100\% \quad (1)$$

$$S_{CO}(\%) = \frac{F_{CO,\text{out}}}{F_{CO,\text{out}} + F_{CO_2,\text{out}}} \times 100\% \quad (2)$$

$$S_{H_2}(\%) = \frac{F_{H_2,\text{out}}}{2\left(F_{CH_4,in} - F_{CH_4,\text{out}}\right)} \times 100\% \quad (3)$$

$$J_{O_2}\left(\text{mL} \cdot \text{min}^{-1} \cdot \text{cm}^{-2}\right) = \frac{F_{O_2}}{S_A} \quad (4)$$

$$F_{O_2} = \frac{1}{2}F_{CO,\text{out}} + F_{CO_2,\text{out}} + \frac{1}{2}F_{H_2O,\text{out}} + F_{O_2,\text{out}} \quad (5)$$

$$F_{H_2O,\text{out}} = 2\left(F_{CH_4,in} - F_{CH_4,\text{out}}\right) - F_{H_2,\text{out}} \quad (6)$$

where F_i is the flow rate of species i, in mL min^{-1}, S_A is the membrane surface area in cm^2. Using the same formula for conversion of CH_4, the H_2 and CO conversions were similarly calculated for the LSCG membrane swept with 50% H_2:CO (in helium) gas mixture.

Carbon balance is in the range of $(100 \pm 10)\%$ and calculated using the following formula

$$\text{Carbon balance} = \frac{F_{CH_4,\text{out}} + F_{CO_\text{out}} + F_{CO_2,\text{out}}}{F_{CH_4.in}} \quad (7)$$

Leakage from GC and valve system was found to be $\sim$0.5% of the O_2 flux and was constant throughout the experiments. The corrected O_2 fluxes were subtracted using the following formula[23]

$$J_{O_2} = \frac{V(x_{O_2} - (21/78)x_{N_2})}{A_m} \quad (8)$$

where V is the permeate gas flow rate (mL·min^{-1}); x_{O2} and x_{N2} are the % concentrations of O_2 and N_2 in the permeate; A_m (cm^2) is the effective membrane area, $A_m = \pi(D_o - D_i)L/\ln\left(\frac{D_o}{D_i}\right)$ where

D_o, D_i, and L are the outer and inner diameter as well as the effective length for oxygen permeation of the hollow fiber membrane, respectively.

Characterization

Characterizations were performed on the LSCG hollow fiber membranes after POM reactions (bare membrane and with catalyst) and after swept with 50% H_2:CO (in helium). The crystalline phase structures of the LSCG hollow fibers were examined using an X-ray powder diffractometer (XRD, Bruker D8), with a Cu target K-α radiation ($\lambda = 0.15406$ nm). The scattering intensities were over an angular range of $20^\circ < 2\theta < 80^\circ$ with scanning speed of 1°min^{-1}. Morphology and structural changes in the hollow fiber membranes were visually observed via a field emission scanning electron microscope coupled to an energy dispersive spectroscopy (FESEM-EDX, Jeol JSM-6700F). The samples were degassed *in vacuo* in order to remove impurities. Platinum coating (ca. 10 nm thickness) was carried out at 20 mA for 40 s.[26]

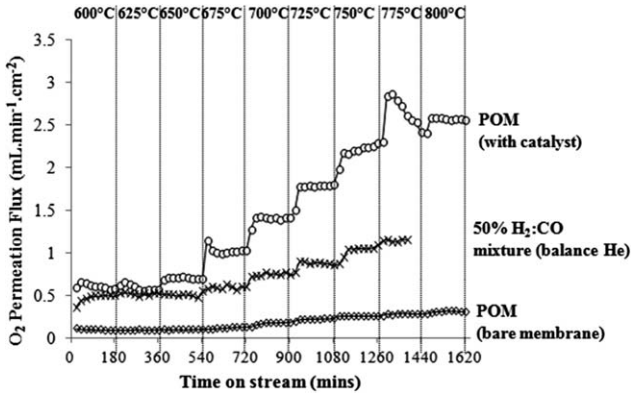

Figure 2. Oxygen permeation flux of LSCG hollow fiber membrane under blank POM with bare membrane, POM with catalyst and with 50%H_2:CO (in He) sweep.

For POM: $F_{air} = 100$ mL·min^{-1}, $F_{CH4} = 2.5$ mL·min^{-1}, $F_{He} = 7.5$ mL·min^{-1} and for 50%H_2:CO: $F_{air} = 100$ mL·min^{-1}, $F_{H2} = 2.5$ mL·min^{-1}, $F_{CO} = 2.5$ mL·min^{-1}, $F_{He} = 5$ mL·min^{-1}.

X-ray photoelectron spectroscopy (XPS) was used to obtain information on the binding energies of the O1s, Sr 3d, Co 2p, and C1s elements in the fresh LSCG membrane for comparison with the membranes after POM reaction as well as exposure to H_2/CO gas. The spectra was obtained via a Kratos AXIS spectrometer with a spatial resolution of 30 μm equipped with a Al K α ($h\upsilon = 1486.6$eV; 1 eV = 1.6302 $\times$ 10^{-19} J) X-ray source. The samples were referenced to the standard calibrated value of the adventitious carbon, C1 s hydrocarbon peak at 284.5 eV prior to fitting the spectrum of samples.

Results and Discussion

Blank POM reaction with bare membrane

The inherent catalytic property of the LSCG hollow fiber membrane was measured first without catalyst in order to elucidate the effect of catalyst in the membrane reactor for the POM reaction. In this blank experiment conducted at the medium temperature of 600 to 800°C, 25% CH_4/He (10 mL min^{-1}) was introduced on the shell side with air flow rate of 100 mL min^{-1} in the lumen side of the membrane reactor. Analysis of the product gas from the GC shows that the main composition of the effluent stream consists of CO_2 and CO as well as unreacted CH_4. Since the steam from the effluent of the membrane reactor is condensed prior to introduction in the GC, therefore, H_2O peak is not detected. On the other hand, H_2 could barely be detected throughout the duration of the reaction.

Figure 2 shows the oxygen permeation fluxes for the blank POM experiment on the bare membrane, catalytic POM reaction and the exposure 50% H_2:CO (in helium) sweep gas. The blank POM experiment on the bare membrane has the lowest O_2 permeation flux at about 0.2 mL $min^{-1}.cm^{-2}$ at 600°C and barely reaching about 0.3 mL $min^{-1}.cm^{-2}$ at 800°C. Based on the POM reaction results shown in Figure 3, it is apparent that the LSCG hollow fiber membrane has inherently poor catalytic activity with a rather low CH_4 conversion of about 2–25% from 600 to 800°C. Furthermore,

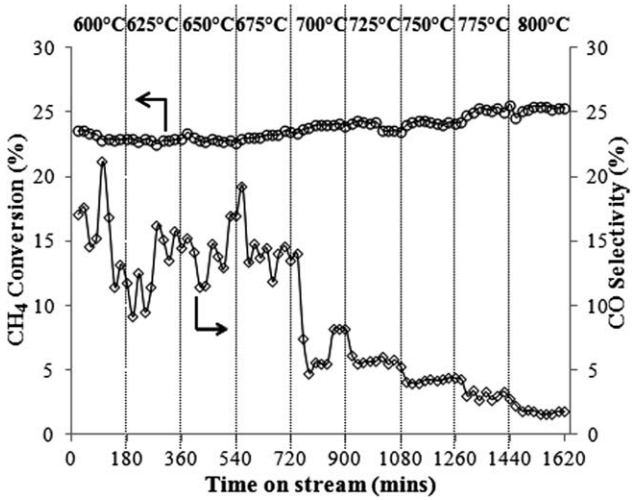

Figure 3. %CH_4 conversion and % CO selectivity for blank POM with bare membrane ($F_{air} = 100$ mL·min^{-1}, $F_{CH4} = 2.5$ mL·min^{-1}, $F_{He} = 7.5$ mL·min^{-1}, $S_A = 1.28$ cm^2).

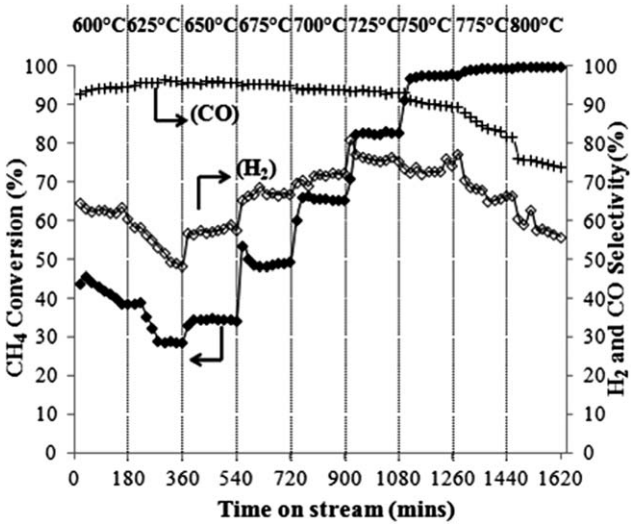

Figure 4. Catalytic performance for POM in membrane reactor ($F_{air} = 100$ mL·min^{-1}, $F_{CH4} = 2.5$ mL·min^{-1}, $F_{He} = 7.5$ mL·min^{-1}, 0.2 g 5%Ni/$LaAlO_3$-Al_2O_3, $S_A = 1.28$ cm^2).

without presence of catalyst, deep oxidation is favored based on the stealthy decrease in CO selectivity from about 17 to 8% at 700°C and after which a rapid decline to about 2% at 800°C. This rapid decline above 700°C is consistent with the obvious increase in O_2 permeation flux from 700°C onward, as shown in Figure 2. O_2 was not detected in the product stream even though there is low conversion of CH_4. In this regard, without the presence of catalyst, oxidation of methane proceeded rather slowly throughout the experiment. This clearly indicates the crucial presence of a suitable catalyst in order to catalyze the reaction.

Hence, in the next section, we provide the results of the catalytic membrane reaction. Generally for POM reactions, Ni based catalysts is the preferable choice, owing to its comparable methane reforming activity with noble metals, wide availability and low cost which is more appealing and practical from an industrial standpoint.[27] As such, we used a methane reforming catalyst developed by our research group (5% Ni/$LaAlO_3$-Al_2O_3) to be packed in the catalytic membrane reactor.

POM reaction in catalytic membrane reactor

The 5% Ni/$LaAlO_3$-Al_2O_3 catalyst was initially reduced at 600°C for 30 min, in order to activate the metallic Ni^0 responsible for providing active sites for the catalytic transformation of methane to syngas in the presence of oxygen. 0.2 g of the prereduced catalyst was then packed in the configuration shown in Figure 1. From the results shown in Figures 2 and 4, presence of the active Ni based catalyst greatly improves the O_2 permeation flux as well as the catalytic activity for POM reaction.

The O_2 permeation flux greatly improved especially from 675°C onward and reached a maximum of about 2.5 mL min^{-1}.cm^{-2} at 800°C. The temperature-accelerated O_2 permeation flux played a major role in improving the CH_4 conversion for the POM reaction. From Figure 4, a slight drop in CH_4 conversion can initially be observed with gradual improvement from 650°C onward. This result correlates with the O_2 permeation flux which shows an increase in flux from 650°C onward. Generally, oxygen surface exchange reaction mechanism becomes activated with increasing temperature. More than 97% of CH_4 conversion is achieved from 750°C onward. This immense improvement in CH_4 conversion is due to the fact that in the presence of catalyst, the selectivity toward H_2 and CO production increases. Hence, at the interface of the catalyst layer on the membrane surface, the presence of highly reducing syngas creates a low-oxygen partial pressure atmosphere. This leads to a large differential pressure gradient across the membrane. According to Zhu et al.[25] oxygen exchange reaction becomes complicated in the presence of catalyst. This is because the reductive unreacted CH_4, as well as product H_2 and CO gases formed from POM reaction on the Ni catalyst, can, through mass-transfer diffusion from catalyst to membrane surface, react with permeated lattice oxygen and adsorbed oxygen species (O^{2-}, O^-, O_2^{2-}, O_2^-, etc.). Likewise, this reaction can also happen with the desorbed gaseous oxygen from the membrane surface. By further removal of the oxygen from the membrane surface (which on its own is rate limiting without the presence of sweep/reactive gases) with the gases from the catalyst bed-interface, this results in increased O_2 permeation for further catalytic conversion to syngas. Therefore, the increase in O_2 permeation flux correlates with the rate of catalytic POM reaction.

However, H_2 selectivity is relatively much lower than CO selectivity especially at temperatures < 675°C. With the increase in temperature, H_2 selectivity increases and reaches a maximum of about 75% at the temperature range of 700 to 750°C. This result correlates with the findings of Yin et al.[28] where significant differences in both H_2 and CO selectivities were observed at the lower temperatures. The continual oxidizing of accumulated carbon at the lower temperature could be a contributing factor in maintaining the markedly higher CO selectivity compared to H_2 selectivity at the lower temperatures.[28] As aforementioned, as the reaction temperature increases, the O_2 flux increases and therefore more CH_4 is consumed. CO product selectivity is above 90% and markedly decreases at temperatures above 750°C onward when the O_2 flow rate (O_2 flux (mL min^{-1}.cm^{-2}) x membrane surface area, (S_A, cm^2)) begins to approach the CH_4 feed flow

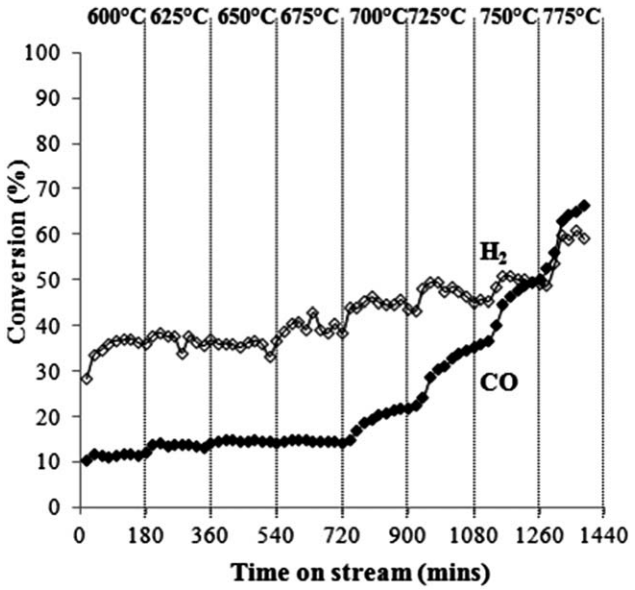

Figure 5. H_2 and CO_2 conversions in membrane exposed to 50% H_2:CO (in He) ($F_{air} = 100$ mL·min$^{-;1}$, $F_{H2} = 2.5$ mL·min^{-1}, $F_{CO} = 2.5$ mL·min^{-1}, $F_{He} = 5$ mL·min^{-1}, $S_A = 1.28$ cm^2).

rate, leading to excess O_2 (O_2:CH_4 >1). Likewise at the temperatures above 750°C, the H_2 selectivity also begins to decline in a similar pace with the decline in CO selectivity in favor of H_2O and CO_2 production from total combustion.

Sweep with 50% H_2 :CO (in helium) gas mixture

Upon exposure to 50% H_2:CO (in helium) as sweep gas, as shown in Figure 2, a noticeable increase in O_2 permeation flux is evident compared to the blank POM reaction with bare membrane. This is due to the presence of strong H_2 and CO reducing gases resulting in enhanced surface reactions, due to immediate conversion of the permeated O_2, resulting in lower O_2 partial pressure, thereby leading to greater driving force.[29,30] The O_2 flux under exposure to 50% H_2:CO (in helium) is comparable to the O_2 flux from the catalytic POM reaction at temperatures lower than 675°C. Above this temperature, the flux begins to increase steadily but at a lower magnitude than the increase in O_2 flux experienced by the catalytic POM reaction. This is because as shown in Figure 4, with increase in temperature, greater catalytic activity in the POM reaction results in greater amount of H_2 production. Stoichiometrically, 1 mol of CH_4 is capable of producing 2 mol of H_2 and 1 mol of CO from subsequent oxidation and reforming reactions. Hence, a greater volumetric flow of the reducing gases are a consequence of the catalytic POM reaction, compared to the equivolume H_2 and CO sweep gas mixture.

Figure 5 shows the %H_2 and %CO conversions from 600 to 775°C. The only reactions that can take place are basically oxidation of the reactants; hence, the equations pertaining to the H_2 and CO conversions are shown as Eqs. 9 and 10 as follows[31]

$$CO + O^{2-} \rightarrow CO_2 + 2e^- \quad (9)$$

$$H_2 + O^{2-} \rightarrow H_2O + 2e^- \quad (10)$$

Due to the steep increment in terms of temperature-accelerated conversions of both H_2 and CO, the immense surface reaction activity and excess water production led to stress and fracture of the membrane at the reactor cold zone near the exit. This disrupted the experiment leading to discontinuation of study just before the last data point could be collected at 775°C. However, the trend can still be observed, whereby it is evident that at lower temperatures (< 700°C), CO oxidation was rather steady with only marginal improvement from 650°C. A dramatic increase in conversion begin to be apparent at the higher temperatures, whereby from 750°C onward, CO conversion begin to surpass H_2 conversion. Generally CO_2 desorption is the rate limiting step in CO oxidation reactions. Furthermore, CO_2 preferentially adsorbs on the perovskite surface to form carbonates such as $SrCO_3$. However, with increasing temperature, these carbonates can easily undergo thermal desorption, hence, with more vacant sites, therefore, the rate for CO oxidation increases as well. Increase in activation of lattice oxygen due to thermal activation of the membrane also contributes to more oxygen vacancy. Increase in oxygen vacancy (especially at temperatures above 750°C) also contributes to increase in selectivity for CO oxidation especially with increasing temperature.[32]

It has been reported that oxidation kinetic sequence in the presence of reducing gases is in the order of $H_2 > CO > CH_4$ and this order correlates with the tendency of the reducing gases to react with surface oxygen ions.[33–35] Our results correlate to this sequence and are distinguished by the H_2 and CO conversions especially in the lower temperatures. However, opposed to previously reported data, this study was conducted in the presence of both H_2 and CO due to their merit of being simultaneously produced during POM reactions. Previous studies were conducted on individual gas exposures and it was shown that for membranes such as $Ba_{0.5}Sr_{0.5}Co_{0.8}Fe_{0.2}O_{3-\delta}$, the membrane material reacts more readily with H_2 compared to CO.[35] From the results shown in Figure 5, this trend is quite evident from the %H_2 and %CO converted at the lower temperatures. As mentioned earlier, with increasing temperature, rate of CO oxidation increases due increase in CO_2 desorption (as surface carbonates), hence, CO conversion increases as well. Also at increasing temperatures, the CO polarization enhances the affinity with perovskite surface, thus, restraining the adsorption of H_2 on the membrane surface.[33]

POM reaction pathways occurring on catalyst surface in catalytic LSCG membrane reactor

Many studies have been devoted in contemplating over the reaction pathways involved in the POM reaction. Two types of main reaction pathways on the catalyst bed as shown below have been generally proposed:[36]

1. direct partial oxidation (DPO) where both CH_4 and O_2 adsorb on the catalyst surface producing H_2 and CO according to reaction (Eq. 9)[37]

$$\textbf{POM}: CH_4 + O_2 \leftrightarrow 2H_2 + CO \quad \Delta H^\circ_{298} = -35\text{kJ/mol} \quad (11)$$

2. combustion-reforming reaction (CRR), where the reactant undergoes complete combustion (Eq. 12), and the resulting water undergoes steam reforming of methane (SRM) (Eq. 13) and CO_2 undergoes dry reforming of methane (DRM) (Eq. 14) as follows[38]

$$\textbf{Total Combustion}: \quad CH_4 + 2O_2 \leftrightarrow CO_2 + 2H_2O \qquad \Delta H^\circ_{298} - 801 \text{ kJ/mol} \tag{12}$$

$$\textbf{SRM}: H_2O + CH_4 \leftrightarrow 3H_2 + CO \qquad \Delta H^\circ_{298} = +206 \text{ kJ/mol} \tag{13}$$

$$\textbf{DRM}: CO_2 + CH_4 \leftrightarrow 2H_2 + 2CO \qquad \Delta H^\circ_{298} = +261 \text{ kJ/mol} \tag{14}$$

It has been generally categorized that at high space velocities ($>10^5$ L.kg^{-1}.h^{-1}), DPO mechanism is favorable and at low space velocities ($<10^5$ L.kg^{-1}.h^{-1}), CRR is more likely to proceed.[39] In this catalytic membrane reactor system, the calculated space velocity is 750 L.kg^{-1}.h^{-1}, and this may indicate that CRR is more likely to take place. Hereby, the lower space velocity requires longer residence times for complete O_2 conversion, allowing more H_2O to adsorb and provide additional adatoms for oxidation of carbon adatoms.[40]

As observed from the results from the oxygen flux from H_2:CO as sweep gas, the O_2 flux begin to increase due to the dramatic increase in CO conversion at temperatures above 700°C alongside with CO conversion to CO_2. Therefore, if direct POM was reaction pathway, the CO and H_2 selectivity should start dropping from 700°C because at this stage, the O_2:CH_4 ratio was more than 0.5 and less than 1. For direct POM reactions, O_2:CH_4 ratio of 0.5 is stoichiometrically advantageous for optimal reaction. However, the temperature region of 700 to 750°C showed the best H_2 and CO selectivities from the catalytic POM reaction. Hence, the reaction pathway at this alludes with the theory of total oxidation followed by reforming with steam and CO_2 produced from the combustion. This was also observed by several other researchers who studied POM in a catalytic membrane reactor.[39,41,42] Even though the H_2 selectivity improves with increasing temperature up to 750°C, however, the H_2 selectivity is still lower than CO selectivity. Therefore, this leads us to believe that a possibility of reverse water gas shift (RWGS) reaction to take place at the same time, since RWGS reaction is prevalent between 700 to 800°C.[43] Furthermore, as discussed earlier for the effect of H_2:CO mixture sweep gas, based on the oxidation kinetic sequence, H_2 is more readily oxidizable to H_2O. Equation 15 following shows the RWGS reaction

$$\textbf{RWGS}: CO_2 + H_2 \leftrightarrow CO + H_2O \qquad \Delta H^\circ_{298} = +41 \text{kJ/mol} \tag{15}$$

Therefore, we summarize later the proposed reaction pathways which take place on the catalyst bed of the LSCG catalytic hollow fiber membrane system during POM in the medium temperature of 600–800°C.

1. Low-temperature region (600–650°C), where O_2 permeation is negligible:

- Methane decomposition on Ni based catalyst (Eq. 16):

$$CH_4 \rightarrow C + 2H_2 \tag{16}$$

- Medium temperature region (650–750°C), where O_2 :$CH_4 < 1$

$$\text{Carbon oxidation}: C_{ads} + O_{ads} \rightarrow CO_{ads} \rightarrow CO \tag{17}$$

- CRR pathway (Eqs. 12–15), in which total combustion is followed by SRM and DRM reactions, proceeds at a higher pace with increasing temperatures due to the endothermic nature of these reactions.
- Simultaneous occurrence of RWGS (700–750°C) (Eq. 15) which is attributed to lower H_2 selectivities compared to CO selectivities.
- Medium — high-temperature region ($>$ 750°C), where O_2:CH_4 >1:
- Increase in dominance of deep oxidation reactions to produce more H_2O and CO_2 as deduced from similar declining pace of H_2 and CO selectivities.

The aforementioned summary can be analogous to general POM reactions which occur in the catalyst bed in catalytic membrane reaction systems. However, temperature shifts can occur depending on the amount of CH_4 feed as well as the permeating ability of the membrane, whereby membranes with better inherent properties can induce permeation at lower temperatures. The catalytic configuration, type and amount also play a role in changing the reaction pathways involved in the catalytic POM membrane reaction systems. In general, CH_4 reacts differently with different catalyst. For example, with an oxidation catalyst, such as another type of perovskite, it is possible that different kinds of oxidation products, such as C_2 and CO_x species could be formed. Hence, the main reaction pathway involved in the POM reaction largely depends on the catalyst property and the membrane material (which determines the oxygen permeation capacity) as well as the temperature regime of the reaction.

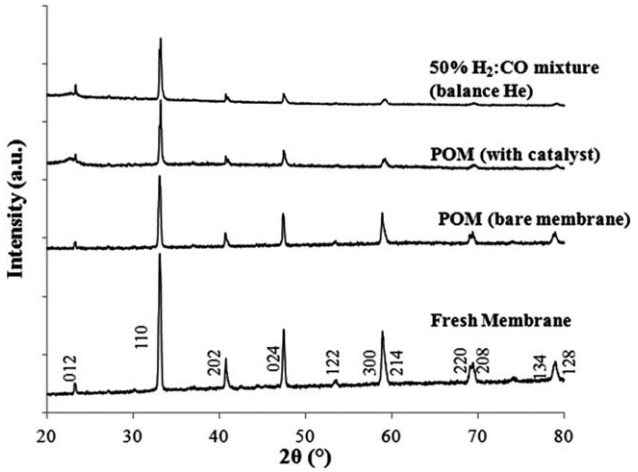

Figure 6. XRD profiles of fresh and postreacted LSCG hollow fiber membranes upon reaction under POM conditions and after 50% H_2:CO (in He) sweep.

Crystalline phase structure analysis

Figure 6 shows the XRD crystalline structure analysis of the LSCG hollow fiber membranes (fresh and postreaction). The standard cubic perovskite phases with the corresponding *d*-spacing values were identified accordingly.[18,44] The only differences between the fresh and postreacted membranes are the reduction in peak intensity as well as slight increase in peak widths. This indicates that deterioration of the initial crystal ordering has taken place to form amorphous debris.[45] Furthermore, the increase in peak widths is indicative of the decrease in crystalline size which may be caused by the decomposition due to the reductive environment. The membrane from the blank POM reaction (without catalyst) has the least crystalline deterioration compared to the membrane

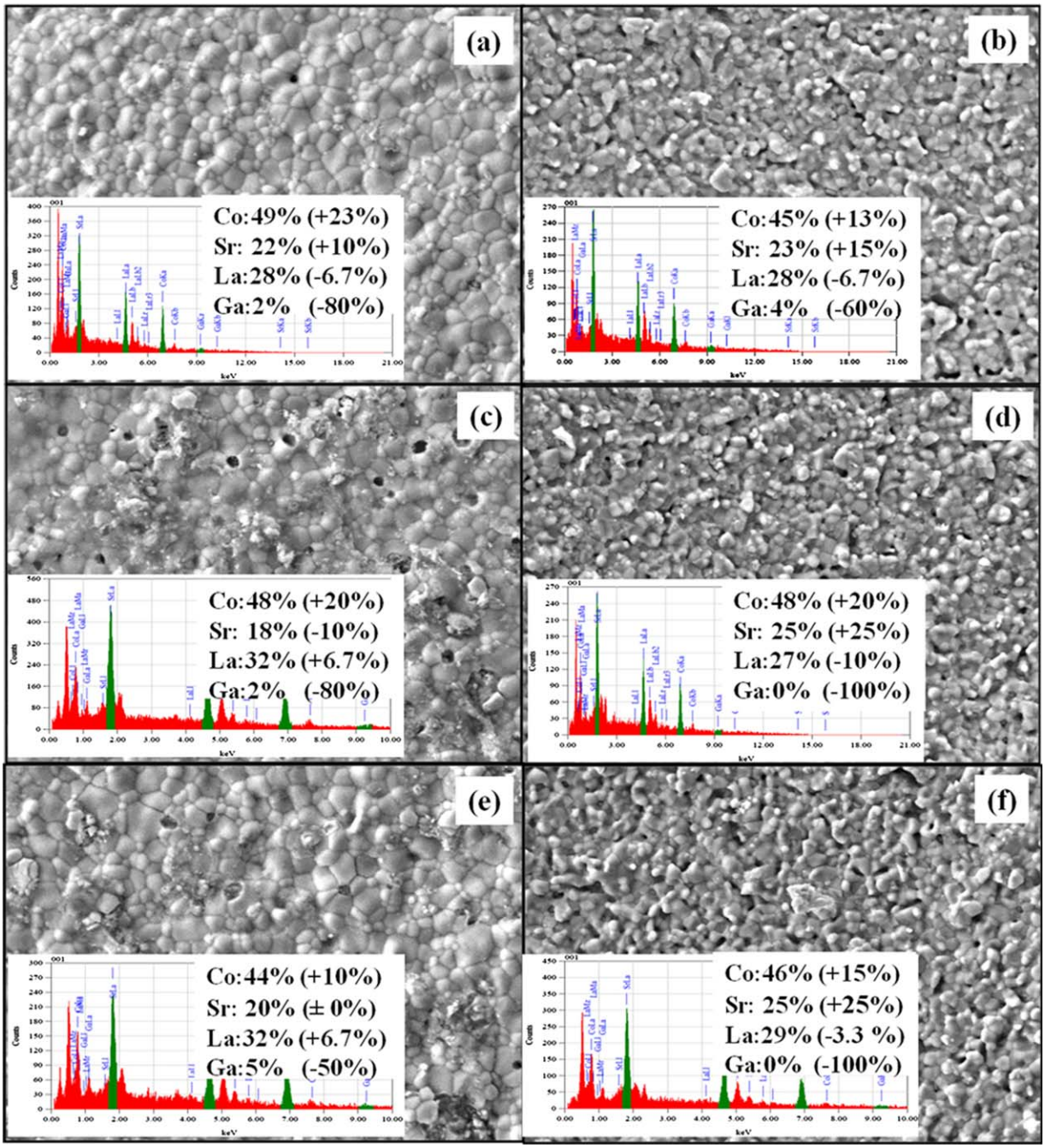

Figure 7. FESEM images of LSCG hollow fiber membranes (inset: EDX summary): (a) external and (b) internal surface after blank POM with bare membrane; (c) external and (d) internal surface after POM with catalyst; and (e) external and (f) internal surface after 50% H_2:CO (in He) sweep.

[Color figure can be viewed in the online issue, which is available at wileyonlinelibrary.com.]

from the catalytic POM reaction as well as the membrane which has been exposed to the 50%H_2:CO mixture (in helium). This is evidently due to the greater concentration gradient imposed on the membrane due to the presence of the reducing gases of H_2, CO compared to just CH_4 only. In order to gain a deeper insight on the composition of these amorphous debris, FESEM-EDX and XPS analysis were conducted and reported as follows.

Surface morphology and elemental distribution via FESEM-EDX

Figure 7 shows the FESEM images with the corresponding EDX spectra for the external (reaction side, left) and internal (air side, right) surfaces of the membrane after blank POM reaction (Figure 7a), catalytic POM reaction (Figure 7b) and exposure to 50% H_2:CO mixture (in helium) (Figure 7c). The values denoted in the brackets after each element show the % difference from the stoichiometric amounts.

Based on morphological observation by FESEM, it can be seen that the changes in the structure and composition of the membrane correlates to the surface reaction activity caused by the presence of reducing gases. In other words, the O_2 permeation flux results correspond to the extent of morphological changes observed on the membrane surface. The surface of Figure 7a is rather intact with isolated lumps present on the surface due to the presence of mainly CH_4 which is

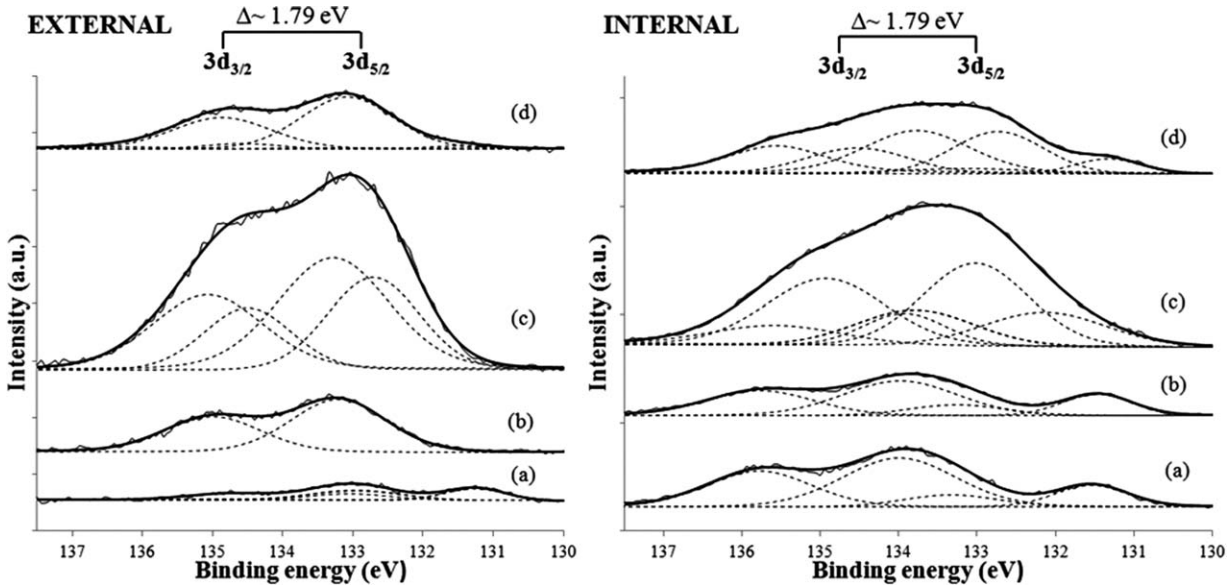

Figure 8. Sr 3d XPS spectra for (a) fresh LSCG membrane, (b) after blank POM with bare membrane, (c) after POM with catalyst, and (d) after 50% H_2:CO (in He) sweep.

the least reducing gas when compared to H_2 and CO. Figure 7b shows the greatest amount of amorphous debris and surface erosion due to the catalytic POM reaction, followed by Figure 7c. The macrovoids on the permeate-interface are opened upon exposure to reducing gases, hence, simultaneously promoting surface exchange kinetics and reducing the membrane effective thickness.[45] On the other hand, no such trend can be distinguished from observation of the internal surfaces of all the postreacted membranes. They all look similar and structurally intact, and the impact of the different surface reactions cannot be differentiated by visual observation of the internal surfaces. The morphological similarity for the internal surfaces of all the postreacted membranes shows that the surface near the reaction side was affected by the reducing atmosphere, while the rest of membrane was stabilized by oxygen transport from air side.[7]

However, corresponding EDX spectral information on the inset of the figures gives more detailed information on the extent of phase segregation. All the samples (both internal and external surfaces) show that Co is present a little in excess. Co-enriched surface phases whose large grains were broken to finer grains have been reported on permeate sides of membrane surfaces due to the erosion caused by the reducing atmosphere.[7,34,46,47] Furthermore, Sr enrichment is observed more clearly on the internal surfaces of all the post reacted membranes. Sr-enrichment in the form of $SrCO_3$ has

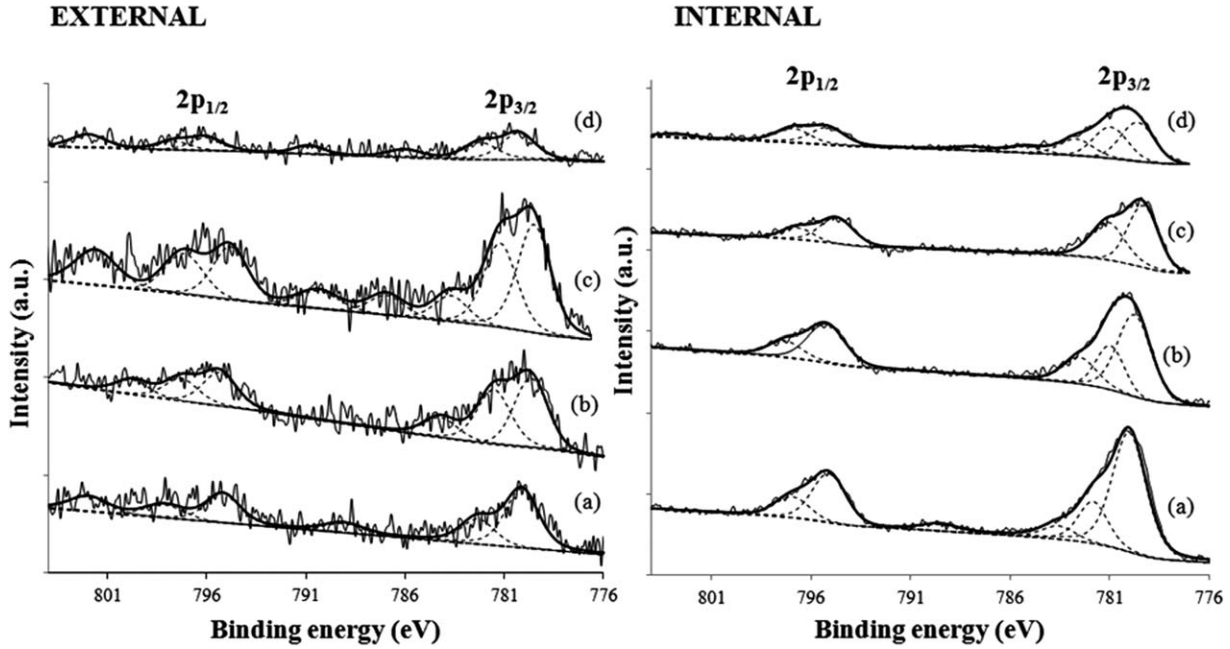

Figure 9. Co 2p XPS spectra for (a) fresh LSCG membrane, (b) after blank POM with bare membrane, (c) after POM with catalyst, and (d) after 50% H_2:CO (in He) sweep.

also been observed by ten Elshof et al.[48] who conducted experiments of oxidative coupling of methane in a $La_{0.6}Sr_{0.4}Co_{0.8}Fe_{0.2}O_3$ membrane reactor.

In general, slight La loss could be observed on all the membrane surfaces with the exception of external surface of membrane after catalytic POM reaction and exposure to H_2/CO mixture in helium, where minor La enrichment is present. On the other hand, Ga deficiency is observed on all the postreacted membranes, especially on the internal surfaces, due to both Co and Sr enrichment. Thus, the La and Ga elements may have tendency to diffuse inwardly toward the membrane bulk. This is due to the intense surface exchange reaction activity which resulted in Sr and Co-enriched phases which have greater mobility to segregate out of the perovskite structure. XPS analysis results are discussed in the next section in order to gain a deeper insight of the segregated Sr and Co elements on the membrane surface.

XPS analysis

As a follow-up from the FESEM-EDX results discussed previously, photoemission spectra was recorded for both the external and internal surfaces of the LSCG hollow fiber membranes before and after reaction. Figure 8 and 9 show the representative Sr3d and Co2p photoemission spectra, respectively, for the fresh LSCG hollow fiber membranes and the postreacted membranes. These spectra are chosen due to their complexities and changeable states especially after reaction under the reducing environment which leads to segregated phases. Table 1 gives a summary of the peaks and the composition of the states for the respective elemental spectra for both the external (reaction side) and internal (air side) surface.

In terms of Sr 3d spectra, as revealed by FESEM-EDX analysis, surface enrichment from Sr can be observed on nearly all the post reacted samples. In order to perform curve fitting for the Sr 3d spectra, a set of criterions were adhered to such as using a splitting energy of 1.79 eV for the Sr doublets, and a Sr $3d_{3/2}$:Sr $3d_{5/2}$ peak area ratio of 2:3.[49] As summarized in Table 1, the lower BE of 131.5–132.1 eV correspond to Sr^{2+} existing in the perovskite structure.[50] At the slightly higher BE values ranging from 132.1–132.7 eV may be due to presence of Sr in the low-oxidation state such as SrO_{1-x} suboxide on the surface.[51] These are basically Sr^{2+} ions surrounded by vacancies in the oxygen-deficient perovskite structure.[52] BE values about 133.0–133.7 eV coincides well with the $SrCO_3$ component.[53,54] The higher BE about 133.8–135.8 eV suggests presence of SrO species.[54,55]

Based on Figure 8 and Table 1, for the fresh LSCG hollow fiber membrane, the external surface shows that the Sr element exists mainly in the form of $SrCO_3$ (due to atmospheric contamination) and Sr^{2+}. The internal surface, however, consists mainly of SrO species with a lesser percentage of Sr^{2+} in the perovskite phase. Upon blank POM reaction (bare membrane), the external surface consists only of $SrCO_3$ species and the internal surface is quite similar to that of the fresh membrane. This is largely due to the CH_4 oxidation activity on the membrane surface, whereby the produced CO_2 reacts with the surface Sr and adsorbs in the form of $SrCO_3$ on the external surface.

On the other hand, presence of $SrCO_3$ carbonate species is more prominent on the LSCG membrane after catalytic POM reaction and exposure to H_2:CO mixture. Even more significantly, for the membrane exposed to the H_2:CO

Table 1. XPS Binding Energy Summary of Sr 3d and Co 2p Elements for Fresh and Post Reacted LSCG Hollow Fiber Membranes

		Fresh Membrane				Blank POM (Bare Membrane)				Catalytic POM (Membrane + Catalyst)				50% H_2:CO (in He) sweep gas			
		Outer		Inner		Outer		Inner		Outer		Inner		Outer		Inner	
Element	State	BE (ev)	Area (%)	BE (ev)	Area (%)	BE (ev)	Area (%)	BE (ev)	Area (%)	BE (ev)	Area (%)	BE (ev)	Area (%)	BE (ev)	Area (%)	BE (ev)	Area (%)
Sr $3d_{5/2}$	Sr^{2+}	131.3	45	131.5	22			131.5	27			132.1	24	131.3	10	131.5	4
	SrO_{1-x}									132.7	39			132.7	41		
	$SrCO_3$	133	55			133.2	100			133.3	61	133	52			133.1	88
	SrO			134	78			133.9	73			133.8	24	133.8	49	134.6	8
Co $2p_{3/2}$	Co^{3+}	780.1	70	780	70	779.7	45	779.7	56	779.5	49	779.3	56	780.3	60	779.6	43
	CoO/Co_3O_4	782.3	30	781.8	22	781.5	40	780.9	24	781.2	39	781.1	44	782.1	40	781	35
	Co^{4+}			783.6	8	784.2	15	782.5	20	783.7	12					782.7	22

mixture, all the $SrCO_3$ exists in the internal surface. Due to the presence of CO, it is well-known that the only reaction that can take place is reaction of CO with the adsorbed O_2 to form CO_2. CO_2 desorption is the rate limiting step from this reaction since it reacts strongly with the Sr to form $SrCO_3$ which adheres more strongly on the internal surface. Even though the membrane from the catalytic POM reaction also has presence of $SrCO_3$, however, due to the effect of catalyst, the formation of CO_2 is suppressed with higher selectivity for CO formation which can desorb more easily compared to the carbonate species. The presence of carbonate on the external surface can also be attributed to the surface contamination. It can also be observed that with presence of both H_2 and CO reducing agents (i.e., from POM catalytic reaction and exposure to H_2:CO mixture), transformation to SrO_{1-x} is more evident. Again, this is ascribed to the intense surface oxygen reaction activity leading to more oxygen vacancies contributed by the presence of these highly reducing gases. However, in all cases, presence of Sr^{2+} in perovskite form especially in the internal surface shows that even in the presence of the Sr-enriched segregates as confirmed by EDX and XPS analysis, the inherent perovskite structure is still maintained, thereby enabling the oxgyen reduction reactions to take place.

In terms of the Co 2p photoemission spectra, XPS analysis provides much insight on the complex Co metal reduction and its state of existence. For the fresh LSCG membrane, as shown in Figure 9a, the Co $2p_{3/2}$ main spectra can be observed about780 eV for both the internal and external surfaces with a weak shake up peak about 789 eV. The presence of the weak shake up peak indicate presence of low-spin Co^{III} corresponding to octahedral Co^{3+}.[56] The corresponding energy difference arising from the Co $2p_{3/2}$ – Co $2p_{1/2}$ splitting of about 15 eV further indicates the presence of Co^{3+}.[57] However, for the external surface of the fresh membrane an additional satellite peak at 802 eV can be observed. Peak deconvolution shows another set of Co $2p_{3/2}$ – Co $2p_{1/2}$ doublets at about 782 and 797 eV, respectively. As summarized in Table 1, the contribution of the Co $2p_{3/2}$ state at the higher binding energy of about 782 eV in the fresh membrane is nearly one-third of total Co element contribution. These peaks can be assigned to Co^{2+} state.[58] Generally, substitution of Sr^{2+} into La^{3+} results in charge imbalances which are compensated by oxidation of Co^{3+} to the Co^{4+}, or by formation of oxygen holes. The Co^{4+} (d^5) ion, however, is not readily stabilized and would be expected to be paramagnetic, giving rise to a shake-up satellite.[59] In order to achieve goodness of fit, the peak at the higher binding energy prior to the satellite region, in the range of 782.5 to 784.2 can be ascribed to Co^{4+}.

During the POM reaction, the reducing nature of the permeate side can cause the membrane to undergo deleterious changes to its surface structure.[55] This leads to enhanced electronic activity due to the hydrocarbon degradation taking place, whereby the strongly reducible nature of Co^{3+} will induce transformation to Co^{2+} which has stable half-filled orbits containing stable electron distribution of $t_{2g}^5 e_g^2$.[60] As can be observed from Figure 9 and Table 1, upon exposure to the reducing gases, the $Co2p_{3/2}$ peak appear to shift to lower binding energies, indicating the presence of Co^{2+}/Co^{3+}. The presence of shake up peaks at 785 and 802 on the external surface of the of the membrane as shown in Figure 9c and 9d confirm the presence of CoO and Co_3O_4 surface oxide species.[61] A shift toward lower BE (ca. 779 eV) have also been observed by Petunchi and Lombardo during reduction of $LaCoO_3$ under H_2.[62] The XPS data correlate with the EDX data shown in Figure 7, and gives greater insight on the elemental existence of the Co-species on the membrane surface.

Conclusions

In this study, medium temperature operation of LSCG catalytic hollow fiber membrane reactor packed with 5%Ni/$LaAlO_3$-Al_2O_3 catalyst has been investigated. Based on the results of blank POM reaction (bare membrane), catalytic POM reaction (membrane with catalyst) and sweep with 50%H_2/CO (in helium), it is evident that with presence of larger amount of H_2 and CO gases, higher oxygen flux can be attained. The oxygen permeation flux from the catalytic membrane reactor reached about 2.5 mL $min^{-1}.cm^{-2}$ compared to only 0.3 mL $min^{-1}.cm^{-2}$ for the blank POM reaction (without catalyst) at 800°C. Based on the catalytic POM reaction, at the optimal temperature of 750°C, CH_4 conversion of 97% is achieved with high H_2 and CO selectivity of about 74 and 91% were obtained. Based on the FESEM-EDX and XPS spectral analysis, presence of $SrCO_3$, CoO and Co_3O_4 can be detected on the external surface of the membrane after catalytic POM reaction, whereas the internal surface of the membrane is enriched with SrO, SrO_{1-x}, CoO and Co_3O_4 phases. Nevertheless, the crystalline perovskite structure and its inherent properties are retained, and, hence, enabling oxygen permeability in the highly reducing environment.

Acknowledgments

The authors gratefully thank the National University of Singapore, National Environmental Agency (NEA-ETRP Grant No.1002114 and RP No. 279-000-333-490) and A*STAR SERC Grant No. 092-138-0022 and RP No. 279-000-292-305) NEA and A*STAR, for generously supporting this work. Yasotha Kathiraser sincerely thanks Dr. Nai-Tao Yang and Mr. Zhigang Wang for technical support and discussion.

Literature Cited

1. Sutthiumporn K, Maneerung T, Kathiraser Y, Kawi S. CO_2 dry reforming of methane over $La_{0.8}Sr_{0.2}Ni_{0.8}M_{0.2}O_3$ perovskite (M=Bi, Co, Cr, Cu, Fe): Roles of lattice oxygen on C—H activation and carbon suppression. *Int J Hydrogen Energy*. 2012;37:11195–11207.
2. Sutthiumporn K, Kawi S. Promotional effect of alkaline earth over Ni-La_2O_3 catalyst for CO_2 reforming of CH_4: Role of surface oxygen species on H_2 production and carbon suppression. *Int J Hydrogen Energy*. 2011;36:14435–14446.
3. Wang W, Ran R, Shao Z. Lithium and lanthanum promoted Ni-Al_2O_3 as an active and highly coking resistant catalyst layer for solid-oxide fuel cells operating on methane. *J Power Sources*. 2011; 196:90–97.
4. Mateos-Pedrero C, Duquesne S, Carrazán SRG, Soria MA, Ruíz P. Influence of the products of the partial oxidation of methane (POM) on the catalytic performances of Rh/Ti-modified support catalysts. *Appl Catal A Gen*. 2011;394:245–256.
5. Li Q, Zhu X, He Y, Yang W. Partial oxidation of methane in $BaCe_{0.1}Co_{0.4}Fe_{0.5}O_{3-\delta}$ membrane reactor. *Catal Today*. 2010;149: 185–190.
6. Balachandran U, Dusek JT, Mieville RL, Poeppel RB, Kleefisch MS, Pei S, Kobylinski TP, Udovich CA, Bose AC. Dense ceramic membranes for partial oxidation of methane to syngas. *Appl Catal A Gen*. 1995;133:19–29.
7. Tsai CY, Dixon AG, Moser WR, Ma YH. Dense perovskite membrane reactors for partial oxidation of methane to syngas. *AIChE J*. 1997;43:2741–2750.

8. Wang H, Feldhoff A, Caro J, Schiestel T, Werth S. Oxygen selective ceramic hollow fiber membranes for partial oxidation of methane. *AIChE J*. 2009;55:2657–2664.
9. Tan X, Li K. Design of mixed conducting ceramic membranes/reactors for the partial oxidation of methane to syngas. *AIChE J*. 2009; 55:2675–2685.
10. Dong H, Shao Z, Xiong G, Tong J, Sheng S, Yang W. Investigation on POM reaction in a new perovskite membrane reactor. *Catal Today*. 2001;67:3–13.
11. Jin W, Li S, Huang P, Xu N, Shi J, Lin YS. Tubular lanthanum cobaltite perovskite-type membrane reactors for partial oxidation of methane to syngas. *J Membr Sci*. 2000;166:13–22.
12. Zhang K, Sunarso J, Shao Z, Zhou W, Sun C, Wang S, Liu S. Research progress and materials selection guidelines on mixed conducting perovskite-type ceramic membranes for oxygen production. *RSC Adv*. 2011;1:1661–1676.
13. Wang H, Tablet C, Feldhoff A, Caro J. Investigation of phase structure, sintering, and permeability of perovskite-type $Ba_{0.5}Sr_{0.5}Co_{0.8}Fe_{0.2}O_{3-\delta}$ membranes. *J Membr Sci*. 2005;262:20–26.
14. Raich BA, Foley HC. Ethanol dehydrogenation with a palladium membrane reactor: An alternative to Wacker chemistry. *Ind Eng Chem Res*. 1998;37:3888–3895.
15. Tan X, Pang Z, Gu Z, Liu S. Catalytic perovskite hollow fibre membrane reactors for methane oxidative coupling. *J Membr Sci*. 2007; 302:109–114.
16. Teraoka Y, Zhang HM, Furukawa S, Yamazoe N. Oxygen permeation through perovksite-type oxides. *Chem Lett*. 1985;11:1743–1746.
17. Sunarso J, Baumann S, Serra JM, Meulenberg WA, Liu S, Lin YS, da Costa JCD. Mixed ionic-electronic conducting (MIEC) ceramic-based membranes for oxygen separation. *J Membr Sci*. 2008;320:13–41.
18. Liang F, Jiang H, Luo H, Caro J, Feldhoff A. Phase stability and permeation behaviour of a dead-end $Ba_{0.5}Sr_{0.5}Co_{0.8}Fe_{0.2}O_{3-\delta}$ tube membrane in high-purity oxygen production. *Chem Mater*. 2011;23: 4765–4772.
19. Yang NT, Kathiraser Y, Kawi S. A new asymmetric $SrCo_{0.8}Fe_{0.1}Ga_{0.1}O_{3-\delta}$ perovskite hollow fiber membrane for stable oxygen permeability under reducing condition. *J Membr Sci*. 2013; 428:78–85.
20. Pei S, Kleefisch MS, Kobylinksi TP, Faber J, Udovich CA, Zhang-McCoy V, Dabrowski B, Balachandran U, Mieville RL, Poeppel RB. Failure mechanisms of ceramic membrane reactors in partial oxidation of methane to synthesis gas. *Catal. Lett*. 1995;30:201–212.
21. Luo H, Tan B, Wei Y, Wang H, Jiang H, Caro J. Oxygen permeability and structural stability of a novel tantalum-doped perovskite $BaCo_{0.7}Fe_{0.2}Ta_{0.1}O_{3-\delta}$. *AIChE J*. 2010;56:604–610.
22. Kharton VV, Tsipis EV, Marozau IP, Yaremchenko AA, Valente AA, Viskup AP, Frade JR, Naumovich EN, Rocha J. Transport and electrocatalytic properties of $La_{0.3}Sr_{0.7}Co_{0.8}Ga_{0.2}O_{3-\delta}$ membranes. *J Solid State Electrochem*. 2005;9:10–20.
23. Kathiraser Y, Wang Z, Yang NT, Zahid S, Kawi S. Oxygen permeation and stability study of $La_{0.6}Sr_{0.4}Co_{0.8}Ga_{0.2}O_{3-\delta}$ (LSCG) hollow fiber membrane with exposure to CO_2, CH_4 and He. *J Membr Sci*. 2013;427:240–249.
24. Wu Z, Wang B, Li K. Functional LSM—ScSZ/NiO—ScSZ dual-layer hollow fibres for partial oxidation of methane. *Int J Hydrogen Energy*. 2011;36:5334–5341.
25. Zhu X, Li Q, He Y, Cong Y, Yang W. Oxygen permeation and partial oxidation of methane in dual-phase membrane reactors. *J Membr Sci*. 2010;360:454–460.
26. Wang Z, Kathiraser Y, Kawi S. High performance oxygen permeable membranes with Nb-doped $BaBi_{0.05}Co_{0.95}O_{3-\delta}$ perovskite oxides. *J Membr Sci*. 2013;431:180–186.
27. Oemar U, Hidajat K, Kawi S. Role of catalyst support over PdO—NiO catalysts on catalyst activity and stability for oxy-CO_2 reforming of methane. *Appl Catal A Gen*. 2011;402:176–187.
28. Yin X, Hong L, Liu Z. Integrating air separation with partial oxidation of methane-A novel configuration of asymmetric tubular ceramic membrane reactor. *J Membr Sci*. 2008;311:89–97.
29. Zhang W, Smit J, Annaland MVS, Kuipers JAM. Feasibility study of a novel membrane reactor for syngas production: Part 1: Experimental study of O_2 permeation through perovskite membranes under reducing and non-reducing atmospheres. *J Membr Sci*. 2007;291:19–32.
30. Zeng Y, Lin YS. Oxidative coupling of methane on improved bismuth oxide membrane reactors. *AIChE J*. 2001;47:436–444.
31. Ikeguchi M, Mimura T, Sekine Y, Kikuchi E, Matsukata M. Reaction and oxygen permeation studies in $Sm_{0.4}Ba_{0.6}Fe_{0.8}Co_{0.2}O_{3-\delta}$ membrane reactor for partial oxidation of methane to syngas. *Appl Cat A Gen*. 2005;290:212–220.
32. Gosavi PV, Biniwale RB. Effective cleanup of CO in hydrogen by PROX over perovskite and mixed oxides. *Int J Hydrogen Energy*. 2012;37:3958–3963.
33. Shen P, Ding W, Zhou Y, Huang S. Reaction mechanism on reduction surface of mixed conductor membrane for H_2 production by coal-gas. *Appl Surf Sci*. 2010;256:5094–5101.
34. Zhang Y, Liu J, Ding W, Lu X. Performance of an oxygen-permeable membrane reactor for partial oxidation of methane in coke oven gas to syngas. *Fuel*. 2011;90:324–330.
35. Jiang Q, Faraji S, Slade DA, Stagg-Williams SM. A review of mixed ionic and electronic conducting ceramic membranes as oxygen sources for high-temperature reactors. *Membr Sci Technol*. 2011;14:235–273.
36. Dissanayake D, Rosynek MP, Kharas KCC, Lunsford JH. Partial oxidation of methane to carbon monoxide and hydrogen over a Ni/Al_2O_3 catalyst. *J Catal*. 1991;132:117–127.
37. Hickman DA, Schmidt LD. Synthesis gas formation by direct oxidation of methane over Pt monoliths. *J Catal*. 1992;138:267–282.
38. Prettre M, Eichner Ch, Perrin M. The catalytic oxidation of methane to carbon monoxide and hydrogen. *Trans Faraday Soc*. 1946;43: 335b–340.
39. Wang H, Cong Y, Yang W. Investigation on the partial oxidation of methane to syngas in a tubular $Ba_{0.5}Sr_{0.5}Co_{0.8}Fe_{0.2}O_{3-\delta}$ membrane reactor. *Catal Today*. 2003;82:157–166.
40. Hickman DA, Schmidt LD. Steps in CH_4 oxidation on Pt and Rh surfaces: High-temperature reactor simulations. *AIChE J*. 1993;39: 1164–1177.
41. Chen CS, Feng SJ, Ran S, Zhu DC, Lin W, Bouwmeester HJM. Conversion of methane to syngas by a membrane-based oxidation-reforming process. *Angew Chem Int Ed*. 2003;42:5106–5112.
42. Caro J, Caspary KJ, Hamel C, Hoting B, Kilsch P, Langanke B, Nassauer K, Schiestel T, Schmidt A, Schomäcker R, Seidel-Morgenstern A, Tsotsas E, Voigt I, Wang H, Warsitz R, Werth S, Wolf A. Catalytic membrane reactors for partial oxidation using perovskite hollow fiber membranes and for partial hydrogenation using a catalytic membrane contactor. *Ind Eng Chem Res*. 2007;46:2286–2294.
43. Fan MS, Abdullah AZ, Bhatia S. Catalytic technology for carbon dioxide reforming of methane to synthesis gas. *ChemCatChem,* 2009;1:192–208.
44. Wang S, Zheng R, Suzuki A, Hashimoto T. Preparation, thermal expansion and electrical conductivity of $La_{0.6}Sr_{0.4}Co_{1-x}Ga_xO_{3-\delta}$ (x = 0.0-0.4) as a new cathode material of SOFC. *Solid State Ionics*. 2004;174:157–162.
45. Tan X, Shi L, Hao G, Meng B, Liu S. $La_{0.7}Sr_{0.3}FeO_{3-\delta}$ perovskite hollow fiber membranes for oxygen permeation and methane conversion. *Sep Purif Technol*. 2012;96:89–97.
46. Gu X, Jin W, Chen C, Xu N, Shi J, Ma YH. YSZ—$SrCo_{0.4}Fe_{0.6}O_{3-\delta}$ membranes for the partial oxidation of methane to syngas. *AIChE J*. 2002;48:2051–2060.
47. Xu SJ, Thomson WJ. Perovskite-type oxide membranes for the oxidative coupling of methane. *AIChE J*. 1997;43:2731–2740.
48. ten Elshof JE, Bouwmeester HJM, Verweij H. Oxidative coupling of methane in a mixed-conducting perovskite membrane reactor. *Appl Catal A Gen*. 1995;130:195–212.
49. van der Heide PAW. Systematic X-ray photoelectron spectroscopic study of $La_{1-x}Sr_x$-based perovskite-type oxides. *Surf Interface Anal*. 2002;33:414–425.
50. Yamazoe N, Teraoka Y, Seiyama T. TPD and XPS study on thermal-behavior of absorbed oxygen in $La_{1-x}Sr_xCoO_3$. *Chem Lett*. 1981;12:1767–1770.
51. Kozhukharov V, Machkova M, Ivanov P, Bouwmeester HJM, Van Doorn R. Surface analysis of doped lanthanide cobalt perovskites by X-ray photoelectron spectroscopy. *J Mater Sci Lett*. 1996;15:1727–1729.
52. Polini R, Falsetti A, Traversa E, Schäf O, Knauth P. Sol-gel synthesis, X-ray photoelectron spectroscopy and electrical conductivity of Co-doped (La, Sr)(Ga, Mg)$O_{3-\delta}$ perovskites. *J Europ Cer Soc*. 2007; 27:4291–4296.
53. Liu B, Zhang Y, Tang L. X-ray photoelectron spectroscopic studies of $Ba_{0.5}Sr_{0.5}Co_{0.8}Fe_{0.2}O_{3-\delta}$ cathode for solid oxide fuel cells. *Int J Hydrogen Energy*. 2009; 34:435–439.

54. Natile MM, Poletto F, Galenda A, Glisenti A, Montinini T, De Rogatis L, Fornasiero P. $La_{0.6}Sr_{0.4}Co_{1-y}Fe_yO_{3-\delta}$ perovskites: Influence of the Co/Fe atomic ratio on properties and catalytic activity toward alcohol steam-reforming. *Chem Mater*. 2008;20:2314–2327.
55. Norman C, Leach C. In situ high temperature X-ray photoelectron spectroscopy study of barium strontium iron cobalt oxide. *J Membr Sci*. 2011;382:158–165.
56. Marcos JA, Buitrago RH, Lombardo EA. Surface chemistry and catalytic activity of $La_{1-y}M_yCoO_3$ perovskite (M = Sr or Th): 1. Bulk and surface reduction studies. *J Catal*. 1987;105:95–106.
57. Natile MM, Ugel E, Maccato C, Glisenti A. $LaCoO_3$:Effect of synthesis conditions on properties and reactivity. *Appl Catal B Environ*. 2007;72:351–362.
58. Prasad DH, Park SY, Oh EO, Ji H, Kim HR, Yoon KJ, Son JW, Lee JH. Synthesis of nano-crystalline $La_{1-x}Sr_xCoO_{3-\delta}$ perovskite oxides by EDTA-citrate complexing process and its catalytic activity for soot oxidation. *Appl Catal A Gen*. 2012;447–448:100–106.
59. Bocquet AE, Chalker P, Dobson JF, Healy PC, Myhra S, Thompson JG. X-ray photoelectron spectra of perovskite-type cobalt oxides $La_{1-x}Sr_xCoO_{3-y}$ ($x = 0_{.4,0.6}$). *Physica C*. 1989;160:252–258.
60. Sun M, Jiang Y, Li F, Xia M, Xue B, Liu D. Dye Degradation Activity and Stability of Perovskite-Type $LaCoO_{3-x}$ ($x = 0$ similar to 0.075). *Mater Trans*. 2010;51:2208–2214.
61. Mota N, Navarro RM, Alvarez-Galvan MC, Al-Zahrani SM, Fierro JLG. Hydrogen production by reforming of diesel fuel over catalysts derived from $LaCo_{1-x}Ru_xO_3$ perovskites: Effect of the partial substitution of Co by Ru (x = 0.01-0.1). *J Power Sources*. 2011;196:9087–9095.
62. Petunchi JO, Lombardo EA. The effect of bulk and surface reduction upon the catalytic behavior of perovskite oxides. *Catal Today*. 1990; 8:201–219.

Manuscript received Jan. 10, 2013, and revision received Mar. 8, 2013.